Inorganic Chemistry

Article

pubs.acs.org/IC

Component Analysis of Dyads Designed for Light-Driven Water Oxidation

Lars Kohler, Nattawut Kaveevivitchai, Ruifa Zong, and Randolph P. Thummel*

Department of Chemistry, University of Houston, 112 Fleming Building, Houston, Texas 77204-5003, United States

Supporting Information

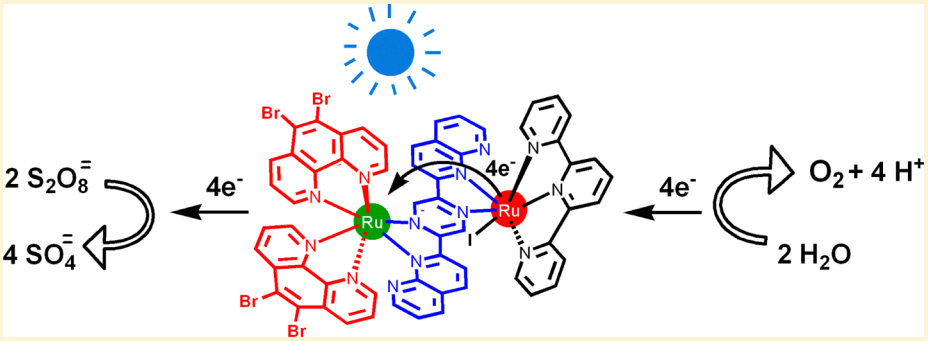

ABSTRACT: A series of seven dyad molecules have been prepared utilizing a $[Ru(tpy)(NN)I]^+$ type oxidation catalyst (NN = 2,5-di(pyrid-2′-yl) pyrazine (**1**), 2,5-di-(1′,8′-dinaphthyrid-2′-yl) pyrazine (**2**), or 4,6-di-(1′,8′-dinaphthyrid-2′-yl) pyrimidine (**3**). The other bidentate site of the bridging ligand was coordinated with 2,2′-bipyridine (bpy), 1,10-phenanthroline (phen), or a substituted derivative. These dinuclear complexes were characterized by their ^{1}H NMR spectra paying special attention to protons held in the vicinity of the electronegative iodide. In one case, **10a**, the complex was also analyzed by single crystal X-ray analysis. The electronic absorption spectra of all the complexes were measured and reported as well as emission properties for the sensitizers. Oxidation and reduction potentials were measured and excited state redox properties were calculated from this data. Turnover numbers, initial rates, and induction periods for oxygen production in the presence of a blue LED light and sodium persulfate as a sacrificial oxidant were measured. Similar experiments were run without irradiation. Dyad performance correlated well with the difference between the excited state reduction potential of the photosensitizer and the ground state oxidation potential of the water oxidation dyad. The most active system was one having 5,6-dibromophen as the auxiliary ligand, and the least active system was the one having 4,4′-dimethylbpy as the auxiliary ligand.

INTRODUCTION

Shifting our energy dependence from fossil fuels to noncarbon based resources, such as hydrogen, holds great promise for the realization of a more sustainable and ecologically sound environment. Current industrial scale production of hydrogen relies on the hydrothermal decomposition of methane or the electrolysis of water. Both processes ultimately utilize fossil fuels as the primary energy source. If we wish to shift this primary source to solar energy, the photochemical decomposition of water into its elements becomes a very attractive approach to clean, abundant energy. This method, often referred to as artificial photosynthesis, is currently impractical because of the lack of an efficient and robust photocatalyst that will use the energy inherent in sunlight to decompose water. In our efforts to develop such a catalyst, we, and others, have made some progress in the oxidative half of the process through the use of both dinuclear[1] and mononuclear complexes of Ru(II).[2]

To catalyze water oxidation, an appropriate Ru(II) complex must be activated by a sacrificial chemical oxidant or the application of an electrochemical potential. The early water oxidation catalysts were often activated by Ce(IV) which readily accepts one electron. To oxidize water to dioxygen, the loss of four electrons from two water molecules is required so that four equivalents of ceric ammonium nitrate would provide one equivalent of O_2. More recently, efforts have been made to avoid the complications inherent in the use of a large excess of ceric ammonium nitrate and also to involve light in the oxidation process. The photoexcited state of $[Ru(bpy)_3]^{2+}$ has an excited state reduction potential that is sufficiently positive to accept an electron from many water oxidation catalysts. Still, a sacrificial electron acceptor, often sodium persulfate or cobalt pentamine chloride, is needed to regenerate the ground state of the photosensitizer.

The next step in improving the efficiency of these photosensitizer-catalyst systems has been to incorporate them both into the same molecule, thus creating a dyad in which an appropriate bridging ligand can link the two key components.[3] We have recently demonstrated that such a dyad system is considerably more effective than a bimolecular system using

Received: September 10, 2013
Published: December 23, 2013

   dx.doi.org/10.1021/ic4022905 | *Inorg. Chem.* 2014, 53, 912−921

Scheme 1. Bridging (1−3) and Auxiliary (4, 5) Ligands Used in This Study

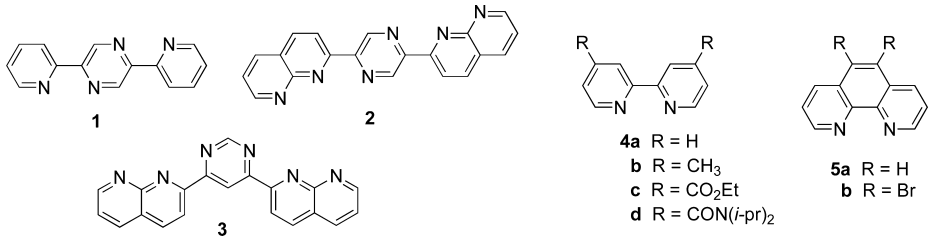

Scheme 2. Preparation of Complexes 7 and 8[a]

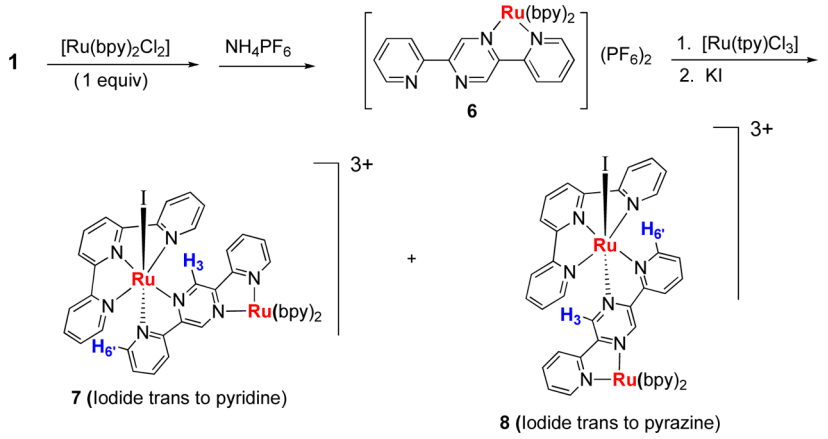

[a]The stereoisomer ratio of **7**:**8** = 3.0 as determined by NMR proton chemical shift analysis of H3 and H6′.

Scheme 3. Preparation of Dyads 10 and 12 as a Single Stereoisomer

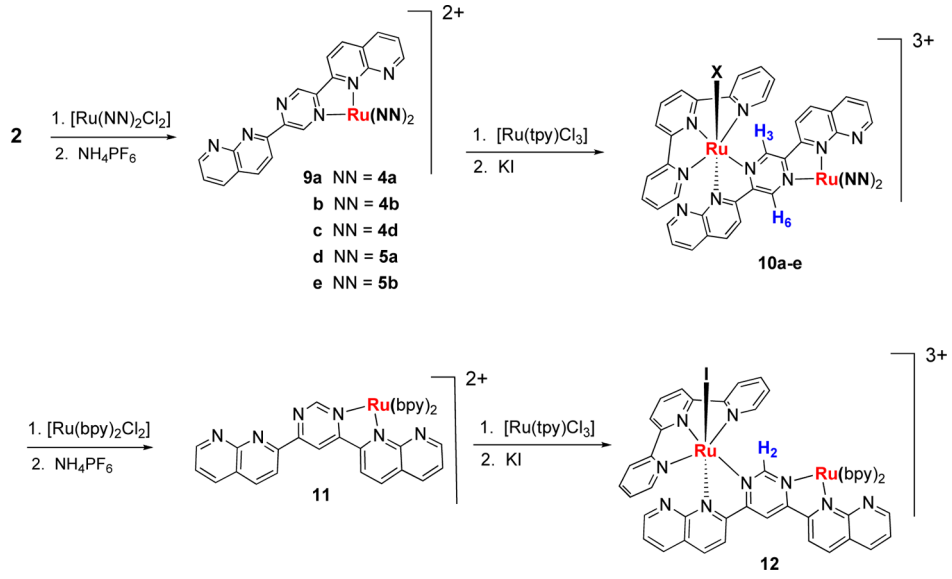

essentially the same sensitizer and catalyst components.[4] As we have done in the past, the present study uses a performance driven synthetic approach to vary the different components of a dyad assembly. We will examine three different but closely related bridging ligands (**1**−**3**) and six different photosensitizers (**4a**−**d** and **5a**,**b**) (Scheme 1). For the water oxidation catalyst, we will employ $[Ru(tpy)(NN)I]^+$ where NN is a bidentate site on the bridging ligand. Earlier work has shown that complexes such as $[Ru(tpy)(bpy)X]^{n+}$ (X = halogen (n = 1) or H_2O (n = 2)) are quite effective water oxidation catalysts.[5]

Synthesis and Characterization. An initial hypothesis was that a more intimate arrangement of the photosensitizer and catalyst sites would be beneficial to the required redox chemistry. Thus we chose pyrazine or pyrimidine as a linker connecting two bidentate sites, creating a situation where only four or five bonds separated the two metal centers and no potentially insulating sp^3 centers intervened. The ligands 2,5-di(pyrid-2′-yl) pyrazine[6] (**1**), 2,5-di-(1′,8′-dinaphthyrid-2′-yl) pyrazine[7] (**2**), and 4,6-di-(1′,8′-dinaphthyrid-2′-yl) pyrimidine[7] (**3**) were prepared according to published methods (Scheme 1). Besides being relatively easy to prepare through Friedländer

dx.doi.org/10.1021/ic4022905 | Inorg. Chem. 2014, 53, 912−921

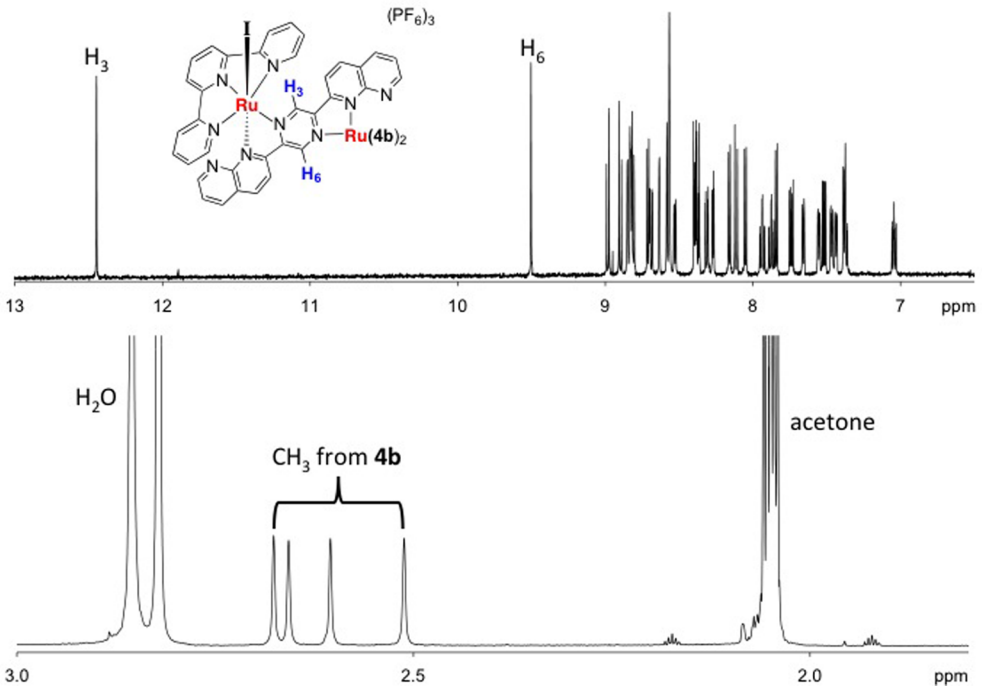

Figure 1. Downfield and upfield region of the ^{1}H NMR spectrum of complex **10b** in acetone-d_6 indicating that the 1,8-naphthyridine moiety is coordinated trans to iodide.

methodology, the incorporation of 1,8-naphthyridine into ligands **2** and **3** provides a binding site that is more electronegative and more delocalized than the pyridine moiety in ligand **1**. Furthermore, the nitrogen that remains unbound to the metal center provides a potential site for mediating proton transfer steps.[8] Ligands **2** and **3** are structural isomers that differ in their connectivity through the central ring (1,3 versus 1,4) and in the directionality of their metal complexation, more or less syn for **3** and anti for **2**. Also ligand **3** shortens the connectivity between the metal centers to four rather than five bonds.

The photosensitizer portion of the dyad was introduced first by treating bridging ligand **1** with one equivalent of $[Ru(bpy)_2Cl_2]$ (bpy = **4a**). Although each of the two bidentate sites in **1** is unsymmetrical, only a single stereoisomer **6** (as a mixture of enantiomers) is formed in this first coordination step.[9] Introduction of the catalyst component of the dyad, however, did present a stereochemical issue. When the complex $[Ru(\mathbf{1})(bpy)_2](PF_6)_2$ is treated with $[Ru(tpy)Cl_3]$ (tpy = 2,2′;6′,2″-terpyridine) two stereoisomers are possible. The pyrazine portion of **1** can bind in the plane of the tpy ligand so that the iodide is trans to the pyridine of **1** (**7**, Scheme 2) or the pyridine can bind in the tpy plane so that the iodide is trans to the pyrazine (**8**). For the bridging ligand **1**, a mixture of stereoisomers is formed, and they can easily be distinguished and identified by ^{1}H NMR. When the axial iodide is trans to pyridine, H3 is held close to the iodide and appears as a strongly deshielded singlet downfield at 11.95 ppm. When the axial iodide is trans to the pyrazine, the H6′ proton on the pyridine ring of **1** is held close to the iodide and appears as a doublet at about 10.65 ppm.

The dyad assemblies involving bridging ligands **2** and **3** were prepared in a similar manner (Scheme 3). The ligand **2** was treated with one equivalent of $[Ru(NN)_2Cl_2]$ where NN is either a bpy derivative **4a, b, d** or a phen derivative **5a,b** to provide the intermediate complexes **9a−e**. These complexes were then treated with $[Ru(tpy)Cl_3]$ followed by KI to exchange chloride for iodide, affording dyads **10a−e** (Scheme 3). The bis(ethoxycarbonyl) bpy derivative where NN = **4c** could not be prepared because the ester moieties were prone to hydrolysis under the aqueous conditions used to convert the iodide to chloride. This observation motivated us to prepare the analogous diamide derivative (NN = **4d**) where the amide function was less susceptible to hydrolysis. A similar sequence with bridging ligand **3**, using $[Ru(bpy)_2Cl_2]$ in the first step provided the dyad **12** in 78% yield.

The NMR characterization of complexes **10a−e** and **12** was simplified in that only a single stereoisomer was formed, having the naphthyridine moiety trans to the iodide. Thus complexes **10a−e** showed H3 as a singlet integrating for one proton in the region from 11.8 to 12.6 ppm as well as a one proton singlet for H6 at 8.8−9.5 ppm. Complex **12** showed a one proton singlet for H2 at 11.05 ppm. In an earlier study of water oxidation catalyzed by the complex $[Ru(tpy)(pynap)(H_2O)]Cl_2$ (pynap = 2-(pyrid-2′-yl)-1,8-naphthyridine) we observed dramatic activity differences between the two stereoisomers of the catalyst. The formation of only a single stereoisomer of complex **10b** is borne out by examination of the ^{1}H NMR spectrum (Figure 1). In the downfield region the peaks are clearly resolved and integrate for a total of 35 protons. The sharp singlets for H3 and H6 are shifted downfield, appearing at 12.45 and 9.50 ppm, respectively. The upfield region of **10b** shows four equal size singlets at 2.51−2.68 ppm, representing the four nonequivalent methyl groups on the two auxiliary ligands **4b**.

In terms of steric hindrance around the binding site, the auxiliary ligands **4b−d** and **5a,b** are quite similar to 2,2′-bipyridine (**4a**, bpy). They differ, however, in electronegativity and in π-electron delocalization. The two methyl groups on **4b** make this ligand a somewhat poorer acceptor than bpy while **4c** with two ethoxycarbonyl groups and **4d** with two carboxamide groups are better acceptors than bpy. The 1,10-phenanthroline

dx.doi.org/10.1021/ic4022905 | *Inorg. Chem.* 2014, 53, 912−921

ligand (**5a**, phen) has a more delocalized π-system than bpy while **5b** is both more delocalized and more electron deficient.

To verify the solution structure of dyad **10a** as determined by NMR, we carried out a single crystal X-ray analysis. The pertinent geometric parameters of this determination are summarized in Table 1, and the X-ray structure of the cation

Table 1. Selected Geometric Parameters for Complex $10a(I)_3 \cdot 4CH_3CN$

	Bond Lengths (Å)		
Ru1−N1	2.096(5)	Ru2−N15	2.031(5)
Ru1−N12	2.048(5)	Ru2−N26	2.101(5)
Ru1−N27	2.071(5)	Ru2−N45	2.075(5)
Ru1−N33	1.977(5)	Ru2−N56	2.049(6)
Ru1−N39	2.067(5)	Ru2−N57	2.069(5)
Ru1−I1	2.710(6)	Ru2−N68	2.066(6)
	Bond Angles (deg)		
N33−Ru1−N12	178.2(2)	N15−Ru2−N56	95.1(2)
N33−Ru1−N39	79.3(3)	N15−Ru2−N68	96.0(2)
N12−Ru1−N39	99.4(2)	N56−Ru2−N68	95.5(2)
N33−Ru1−N27	79.1(2)	N15−Ru2−N57	93.8(2)
N12−Ru1−N27	102.2(2)	N56−Ru2−N57	169.9(2)
N39−Ru1−N27	158.2(2)	N68−Ru2−N57	78.7(2)
N33−Ru1−N1	101.08(19)	N15−Ru2−N45	174.6(2)
N12−Ru1−N1	77.69(18)	N56−Ru2−N45	79.6(2)
N39−Ru1−N1	91.9(2)	N68−Ru2−N45	84.9(3)
N27−Ru1−N1	94.99(19)	N57−Ru2−N45	91.5(2)
N33−Ru1−I1	85.94(14)	N15−Ru2−N26	77.81(18)
N12−Ru1−I1	95.21(13)	N56−Ru2−N26	88.2(2)
N39−Ru1−I1	85.47(15)	N68−Ru2−N26	173.1(2)
N27−Ru1−I1	90.17(14)	N57−Ru2−N26	98.4(2)
N1−Ru1−I1	171.96(13)	N45−RuZ2−N26	101.5(2)
	Dihedral Angles (deg)		
N1−C10−C11−N12	−6.1(8)	N45−C50−C51−N56	−3.3(9)
C9−C10−C11−N12	176.5(6)	C49−C50−C51−N56	178.9(7)
N1−C10−C11−C16	169.1(6)	N45−C50−C51−C52	176.7(7)
C9−C10−C11−C16	−8.3(10)	C49−C50−C51−C52	−1.1(12)
C13−C14−C17−N26	171.2(6)	N27−C32−C34−N33	1.7(8)
N15−C14−C17−N26	−5.5(8)	C31−C32−C34−N33	−179.6(6)
C13−C14−C17−C18	−6.6(10)	N27−C32−C34−C35	−176.1(6)
N15−C14−C17−C18	176.8(6)	C31−C32−C34−C35	2.6(11)
N57−C62−C63−C64	−174.2(7)	N33−C38−C40−N39	1.3(8)
C61−C62−C63−C64	7.3(12)	C37−C38−C40−N39	179.5(7)
N57−C62−C63−N68	3.4(9)	N33−C38−C40−C41	−177.8(6)
C61−C62−C63−N68	−175.2(7)	C37−C38−C40−C41	0.5(11)

of **10a** is shown in Figure 2A. The Ru−N bond lengths involving the terpyridine and the two bipyridine ligands are within the normal range of what is expected for such bonds. The shortest Ru−N bond involves the central pyridine ring of tpy (1.98 Å). The two ruthenium ions are not symmetrically bound to the two bidentate sites of the bridging ligand. The Ru−N bonds involving the central pyrazine rings are considerably shorter (2.03 and 2.05 Å) than the Ru−N bonds involving the peripheral 1,8-naphthyridine rings (both 2.10 Å). The Ru−I bond (2.71 Å) is the longest one in the molecule. The N−Ru−N bond angles interior to the five-membered chelate rings involving the bpy and tpy ligands fall in the narrow expected range of 78.7−79.6°. The N33−Ru1−N12 angle of 178.2° indicates that the tpy is linearly oriented with regard to the central pyrazine. If one considers the dihedral angles involving the interpyridine bonds, these fall in the range

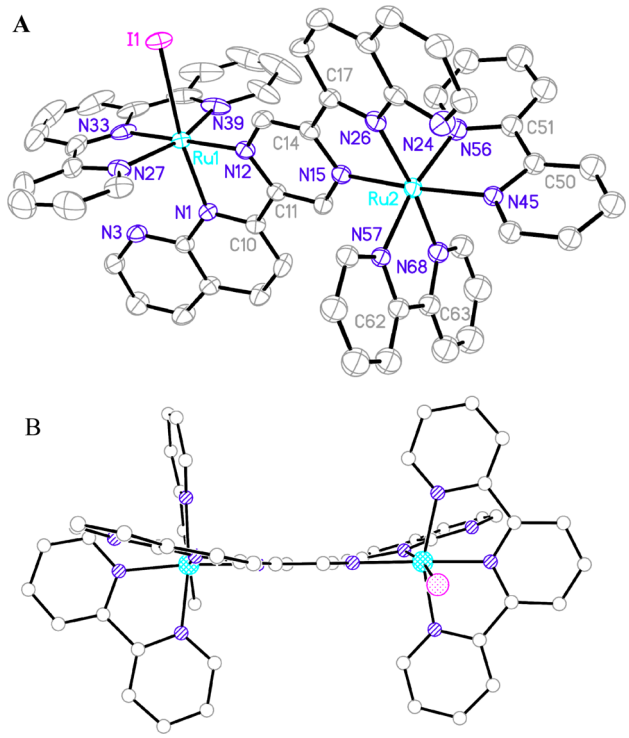

Figure 2. (A) Perspective view of the cation of **10a** with 50% probability thermal ellipsoids and atomic numbering scheme. Hydrogens have been omitted for clarity. (B) Ball and stick view of the cation of **10a** from a vantage point perpendicular to the approximate plane of the tpy ligand.

of 1.1−2.2° except for the bpy containing N57 and N68 where this angle is 5.3°. The dihedral angles about the pyrazine-naphthyridine bonds are less planar at 6.0 and 7.2°.

One interesting feature of this structure is that the bridging ligand is bowed. This distortion becomes apparent as we view the molecule from a vantage point perpendicular to the approximate plane of the tpy ligand (Figure 2B). This bowing could, in part, result from electrostatic repulsion between the nonbonded nitrogens of the 1,8-naphthyrine rings (N3 and N24) and the N33 of tpy (N3−N33 = 2.81 Å) and the N45 of bpy (N24−N45 = 2.84 Å).

Spectroscopic and Electrochemical Properties. Table 2 summarizes the electronic absorption, emission and electrochemical data measured for the prepared dyads and their precursor mononuclear complexes possessing only the sensitizer component. The visible absorption spectra of the sensitizer complexes **9a−e** are illustrated in Figure 3. These spectra consist of two broad, long wavelength, well separated bands that are associated with an excited state metal-to-ligand charge transfer (MLCT) absorption. The high energy band appears in the range of 424−444 nm and is associated with charge transfer from an Ru($d\pi$) to a bpy or phen(π^*) orbital. The two sensitizers having electronegative substituents, the 4,4′-bpy diamide **9c** and the 5,6-dibromophen **9e** show the strongest absorption, appearing at slightly lower energy. The long wavelength band is associated with charge transfer from an Ru($d\pi$) to a ligand **2** (π^*) orbital, and the lower energy of this absorption as compared to the Ru($d\pi$) to bpy or phen(π^*) band is associated with the much more electronegative character of the bridging ligand. For **9c** and **9e** this band is slightly blue-shifted appearing at 540 and 529 nm, respectively.

dx.doi.org/10.1021/ic4022905 | *Inorg. Chem.* 2014, 53, 912−921

Table 2. Electronic Absorption, Emission, and Ground and Excited State Electrochemical Potential Data

compound	λ_{max} (log ε)[a]	$\lambda_{emission}$ (77 K)[b]	$E_{1/2}^{ox}$ (ΔE)[c]	$E_{1/2}^{red}$ (ΔE)[c]	$E^*_{1/2}{}^{red}$[d]	$E^*_{1/2}{}^{ox}$[d]
$[Ru(bpy)_3]^{2+}$	453 (4.16)		1.27 (84)[e]	−1.34 (73)[e]	0.77[e]	−0.81[e]
6	486 (3.72)[f]	647[f]	1.33[f]	−1.03, −1.52[f]	0.89	−0.59
7/8	441 (4.12), 608 (4.24)		0.99 (95), 1.60ir	−0.66 (77), −1.19 (85)		
9a	427 (3.92), 543 (3.81)[g]	765	1.40[g]	−0.63, −1.06[g]	0.99	−0.22
9b	424 (3.94) 561 (3.78)	795	1.27 (67)	−0.70 (83), −1.13 (83)	0.86	−0.27
9c	444 (4.10), 540 (3.94)	739	1.41 (86)	−0.67 (69), −1.08 (68)	1.01	−0.27
9d	424 (4.03) 545 (3.85)	750	1.40 (71)	−0.66 (82), −1.05 (133)	0.99	−0.25
9e	435 (4.12), 529 (3.96)	724	1.54 (110)	−0.63 (75), −1.09ir	1.09	−0.18
10a	439 (4.09), 481 (4.12), 684 (4.10)		0.93 (94), 1.52ir	−0.44 (76), −0.80 (84)		
10b	442 (4.25), 486 (4.28), 692 (4.27)		0.97 (67), 1.49ir	−0.41 (70), −0.77 (71)		
10c	459 (4.44), 473 (4.42), 674 (4.31)		0.94 (98), 1.66ir	−0.43 (70), −0.77 (66)		
10d	435 (4.27) 481 (4.26), 683 (4.26)		0.95 (77), 1.59ir	−0.43 (67), −0.78 (52)		
10e	451 (4.42), 468 (4.40), 667 (4.28)		0.94 (75), 1.64ir	−0.43 (73), −0.76 (98)		
11	431 (4.13), 559 (4.03)[g]	773	1.34[g]	−0.62, −1.12[g]	0.99	−0.27
12	436 (4.08), 586 (3.91), 676 (3.87)		0.95 (122), 1.56ir	−0.45 (86), −0.89 (99)		

[a]Measured in H_2O/CH_3CN (4:1) (5.0×10^{-5} M) at 20 °C; λ in nm and log ε in L·mol^{-1}·cm^{-1}. [b]Measured in ethanol/methanol (4:1) rigid matrix at 77 K; excitation at absorption maxima; λ in nm. [c]Measured with a glassy-carbon electrode at 100 mV/s in CH_3CN containing 0.1 M NBu_4PF_6 and $E_{1/2}$ reported in volts relative to SCE; $E_{1/2}$ = (Epa + Epc)/2 in volts, and ΔE = (Epa − Epc) in mV; ir = irreversible. [d]Calculated using $E^*_{1/2}{}^{ox} = E_{1/2}{}^{ox} - E_{em}$ and $E^*_{1/2}{}^{red} = E_{1/2}{}^{red} + E_{em}$; E_{em} estimated using the emission maxima at 77 K. [e]Reference 10. [f]Reference 11. [g]Reference 7.

It is noteworthy that the absorption for the poorest acceptor, the dimethyl bpy complex **9b**, is the most red-shifted.

When the second Ru(II) is introduced as $[Ru(tpy)I]^+$ into the vacant bidentate site of the sensitizer complexes **9a−e**, a dramatic change occurs in the absorption spectra (Figure 4). The absorption at shorter wavelength now shows two fairly well resolved bands. Compared to the similar band for **9a−e**, these two bands are slightly red-shifted. These two bands are attributed to MLCT from Ru to either the auxiliary bidentate (**4** or **5**) or the tpy ligand. The absorptions in the range of 529−561 nm have completely disappeared and been replaced by a broad band having three poorly resolved components centered at 667−692 nm. The most intense absorptions are again the ones associated with the bpy-diamide and dibromophen ligands, **10c** and **10e**.

The sensitizer based on the pyrimidine linker **11** shows absorption properties that are quite similar to the analogous pyrazine-based sensitizer **9a** indicating that the nature of this central linker, pyrimidine vs pyrazine, is less important in determining overall photophysical properties.

The sensitizer complexes, **6**, **9a−e**, and **11** were essentially nonemissive at room temperature but did show emission at 77 K in a EtOH/MeOH (4:1) glass. The systems involving a 1,8-naphthyridine ring emitted in the range of 724−795 nm while the dipyridylpyrazine complex **6** emitted at 647 nm. These values were used to estimate the excited state redox properties of the photosensitizers. We attempted to measure the emission

dx.doi.org/10.1021/ic4022905 | Inorg. Chem. 2014, 53, 912−921

spectra for the dyads **10a**, **b**, and **e** at 77 K. Exciting at the lowest energy absorption, we were unable to see any significant emission.

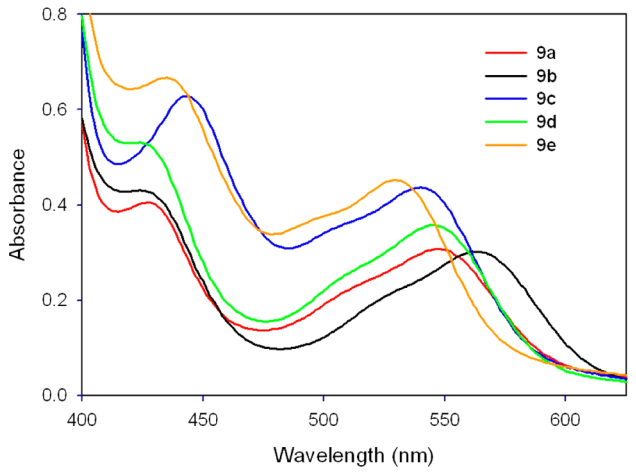

Figure 3. Electronic absorption spectra of **9a–e** in H_2O/CH_3CN (4:1) (5.0×10^{-5} M).

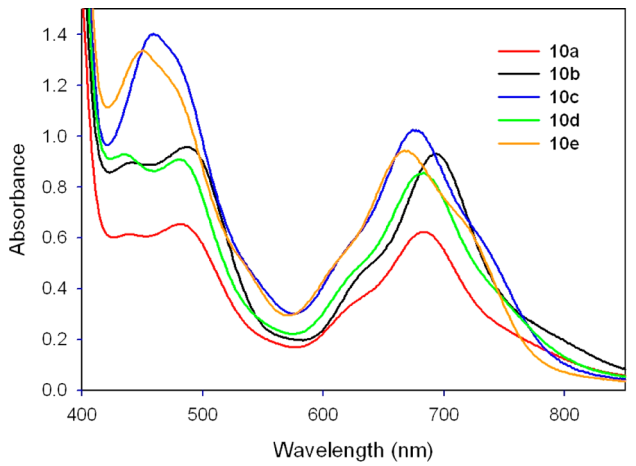

Figure 4. Electronic absorption spectra of **10a–e** in H_2O/CH_3CN (4:1) (5.0×10^{-5} M).

With regard to electrochemical redox properties, these complexes showed an oxidation wave that was associated with the removal of an electron from a metal-based d-orbital and a reduction wave that corresponded to the addition of an electron to the π^* orbital of the most electronegative ligand. Where a second oxidation wave could be observed, it was irreversible in character while nearly all the reduction waves show good reversibility. The sensitizer molecules $[Ru(bpy)_3]^{2+}$, **6**, **9a**, and **11** all contain the $[Ru(bpy)_2]$ fragment bound to a third bidentate ligand. The oxidation potential for these systems does not vary much, ranging from +1.27 V for the $[Ru(bpy)_3]^{2+}$ complex to +1.40 V for **9a**. Changing the nature of the auxiliary bpy ligand from **9a–9e** caused some variation from +1.27 V to +1.54 V with dimethylbpy and dibromophen representing the two extremes, respectively. There was considerably less variation in the oxidation potentials of the dyads **10a–e** which ranged from 0.93 to 0.97 V, indicating that it is considerably easier to remove an electron from the dinuclear complexes. The reduction potentials, that are ligand-based, show considerably more variation. As one goes from $[Ru(bpy)_3]^{2+}$ to **6** to **9a**, to **11**, the reduction potential increases from −1.34 V to −0.62 V reflecting the fact that it is much easier for the bridging ligands to accept an electron, and this is particularly true for the naphthyridine containing sensitizers **9a** and **11**. Variation of the auxiliary ligand in the sensitizer **9a–e** has little effect on the reduction potential that varies from −0.63 to −0.70 V. The same is true for the dyads based on **10** that vary from −0.41 to −0.44 V.

Water Oxidation. The objective of this study is to evaluate and understand the importance of the various components that make up a light-driven water oxidation dyad. Table 3 summarizes the water oxidation data collected for the seven dyads presented in this work. The first three columns report the thermodynamic data (TON), the kinetic data measured as initial rates, and the induction period observed prior to oxygen evolution. We use sodium persulfate as a sacrificial electron acceptor in this work. The reduction of sodium persulfate occurs at a potential of 2.12 V and the initially formed sulfate radical has an even higher potential of 2.6 V. Both these species are sufficiently strong oxidants to oxidize water but, kinetically, this reaction is very slow. The last two columns of Table 3 show the initial rate for the dark reaction utilizing sodium persulfate and the dyad and the prerequisite induction period. For the dark reaction the initial rates fall in the fairly close range of 18 ± 6 to 31 ± 5 × 10^{-4} μmol/min, and the induction periods vary from 960 to 1740 s. In comparing the light-driven data for the target systems to the dark data, it becomes quite apparent that system **10b** is essentially ineffective as a photosensitized dyad, and we are probably just observing a dark persulfate oxidation of the catalyst leading to a small amount of oxygen. The other light-driven dyad data all fall within a fairly close range, but the observed trends are meaningful and consistent with theory (Figure 5).

Table 3. Water Oxidation Data for Dyads

cmpd	TON (1 h)	initial rate (10^{-4} μmol/min) blue light	induction period (sec)	initial rate (10^{-4} μmol/min) dark expt.	induction period (sec) dark expt.[a]
7	66	64 ± 9	30	30 ± 3	1080
10a	35	54 ± 6	20	26 ± 5	1020
10b	20	30 ± 9	1040	20 ± 3	1080
10c	47	57 ± 3	220	31 ± 5	960
10d	50	62 ± 5	20	18 ± 6	1200
10e	68	75 ± 9	20	28 ± 7	1740
12	48	60 ± 8	50	19 ± 5	1200

[a]Although persulfate is thermodynamically capable of oxidizing water this reaction is kinetically slow. Thus the dark reaction, which presumably takes place through the direct action of persulfate on the catalyst, requires a long induction period.

The sensitizer portion of the dyad must have an excited state reduction potential that is sufficiently positive so that it can oxidize the catalyst part of the dyad. The greater this potential difference the more efficient the dyad. In the case of dyad **10b**, the potential difference is −0.09 V and thus the photooxidized sensitizer cannot drive the catalyst and the system is essentially inactive as a light-driven dyad. For dyad **10e**, on the other hand, the potential difference is 0.15 V, and this dyad shows the fastest rate and the highest turnover number. Dyads **10a** and **10c** have similar potential differences +0.06 and +0.07 V, and their initial rates are very similar at 54 ± 6 and 57 ± 3 × 10^{-4}μmol/min. The induction period for **10c** seems a bit long

dx.doi.org/10.1021/ic4022905 | Inorg. Chem. 2014, 53, 912–921

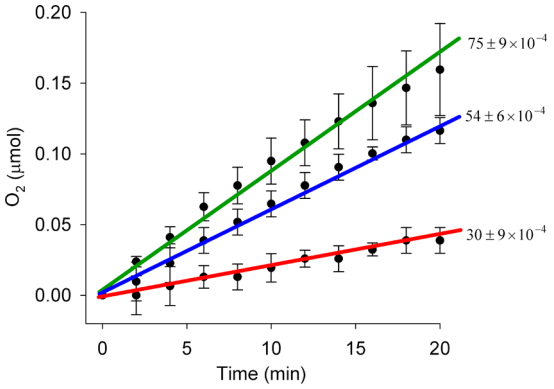

Figure 5. Initial rate (μmol/min with error bars) of oxygen evolution measured after the induction period for dyads **10b** (red), **10a** (blue), and **10e** (green).

(220 s), but one should also note that this system has the fastest dark rate and shortest dark induction period.

In comparing the three different bridging ligands, **1**−**3**, there does not appear to be any significant difference in the performance of their respective dyads. The initial rate data for **7**, **10a**, and **12** are essentially identical. The central linker of the bridging ligand does not appear to make much difference, being pyrazine for **7** and **10** and pyrimidine for **12**. The same analysis holds for the peripheral binding unit of the bridging ligand, being either pyridine or 1,8-naphthyridine.

CONCLUSIONS

Three different bis-bidentate bridging ligands were synthesized based on either a pyrazine or a pyrimidine core. Two 2-pyridyl or 1,8-naphthyrid-2-yl groups were appended to this core so as to create two separate but highly integrated binding pockets. One of these binding pockets was coordinated with a $Ru(NN)_2$ subunit to act as a photosensitizing component (NN = bpy, phen, or a disubstituted derivative). The other binding pocket was coordinated with [Ru(tpy)I] to create a water oxidation catalyst. These dyads were characterized by their ^{1}H NMR spectra, as well as their electronic absorption, emission, and electrochemical properties. Seven dyads were evaluated for their ability to catalyze the oxidation of water when subjected to blue LED irradiation in the presence of sodium persulfate as a sacrificial oxidant. The TONs and initial rates of O_2 production were measured as well as the induction period required before the commencement of oxygen evolution. The least active system was **10b** where NN = 4,4′-dimethylbpy, which was essentially inactive, and the most active system was **10e** where NN = 5,6-dibromophen.

Dyad activity is explained by a consideration of the excited state potential of the sensitizer portion of the molecule that must be greater than the ground state oxidation potential of the dyad so that it can accept an electron from the catalyst portion. The greater this energy difference, the stronger the driving force and the more effective the dyad is at catalyzing light-driven water oxidation. The measured TONs and initial rates are modest. The initial supposition that an intimate arrangement of the photosensitizer and catalyst sites would be beneficial may not be well founded. Fast forward charge transfer in one direction, aided by the intimate ligand arrangement, may be thwarted by equally facile charge transfer in the reverse direction. Future studies will be directed toward dyad systems where the sensitizer and catalyst sites are still linked but in a less intimate and more controlled fashion.

EXPERIMENTAL SECTION

The ^{1}H NMR spectra were recorded at room temperature on JEOL ECX-400 and ECA-500 spectrometers operating at 400 and 500 MHz. Chemical shifts are reported in parts per million (ppm) referenced to the residual solvent peak. The J values are ±0.5 Hz. Electronic absorption spectra were recorded with a VARIAN Cary-50 UV−visible spectrophotometer and were corrected for the background spectrum of the solvent. Emission spectra were obtained on a Perkin-Elmer LS-50B luminescence spectrometer equipped with a Hamamatsu R928HA photomultiplier tube. Electrochemical measurements were carried out using a BAS Epsilon electroanalytical system. Cyclic voltammetry (CV) experiments were performed at room temperature in a one-compartment cell equipped with a glassy carbon working electrode, a saturated calomel reference electrode (SCE), and a Pt wire as the auxiliary electrode in CH_3CN containing tetrabutylammonium hexafluorophosphate (0.1 M) at a scan rate of 100 mV s^{-1}. The microwave (MW) reactions were carried out in a household MW oven modified according to a published description.[12] Elemental analyses were performed by QTI, P.O. Box 470, Whitehouse, NJ 08888. All reagents and solvents were purchased from commercial sources and were used as received except the 2,5-(1′,8′-naphthyrid-2′-yl)pyrazine,[7] $[Ru(tpy)Cl_3]$,[13] $[Ru(\mathbf{4b})_2Cl_2]$,[14] $[Ru(\mathbf{4c})_2Cl_2]$,[15] $[Ru(\mathbf{4d})_2Cl_2]$,[15] $[Ru(\mathbf{5a})_2Cl_2]$,[14] $[Ru(\mathbf{5b})_2Cl_2]$,[14] **6**[9], and **9a**[7] that were prepared according to published procedures.

Oxygen Measurement. A 2-necked flask, fitted with a septum cap and a YSI 5331A oxygen probe connected to a YSI 5300A biological oxygen monitor, is charged with a $Na_2SiF_6/NaHCO_3$ buffer at pH 5.3 ± 0.2 and $Na_2S_2O_8$ (9.4 mg, 0.04 mmol).[16] Before each experiment a fresh Teflon membrane was installed over the YSI probe tip, and the probe was calibrated in oxygen-free (N_2 purge) and oxygen saturated (O_2 purge) water. The calibration was adjusted to give a reading of 19 ± 1% O_2 for air saturated water. The mixture solution was purged with N_2 to provide an oxygen-free solution and then the dyad (6.25×10^{-6} mmol) in acetonitrile (50 μL) was introduced by syringe through the septum cap. The program "Bytewedge" (Fog Software, Inc., fogsoft.com) gave an O_2 reading every 10 s. The initial rates of oxygen evolution (μmol·min^{-1}) were calculated from the plot of oxygen evolution as a function of time and reported as the average value from three separate measurements along with the standard deviation. The turnover number was determined by using a YSI 5331A oxygen probe immersed in the solution.

The 18 module blue LED light strip and a 12 V DC power source were obtained from Creative Lighting Solutions (www.CreativeLightings.com): product code CL-FRS-1212IN-RGB. Each LED module consists of 3 light sources, and the module was wired to allow the illumination of all 3 sources. The strip was wrapped around a water jacketed beaker containing the reaction vessel and adjusted to 20 °C, covered with aluminum foil, and illuminated for the time indicated.

Synthesis of ***7*** *and* ***8****.* A mixture of **6** (125 mg, 0.133 mmol) and [Ru(tpy)Cl$_3$] (59 mg, 0.133 mmol) in EtOH/water (3:1, 20 mL) in the presence of triethylamine (0.5 mL) was refluxed for 2 d. After reducing the volume, NH_4PF_6 (200 mg) dissolved in water was added. The precipitate was filtered, washed with water, and dried. Chromatography on alumina, eluting first with acetone and then acetone/KPF_6, followed by a second chromatography on silica, eluting with acetone/KPF_6 and recrystallization from acetone/water afforded the chloro-complex, a dark green solid (65 mg, 34%), as a mixture of two isomers, involving the Ru−Cl bond relative to the bridging ligand. This chloro-complex (65 mg, 0.045 mmol) and KI (149 mg, 0.895 mmol) in acetone/water (1:1, 15 mL) was heated at 90 °C for 2 d. After reducing the volume, NH_4PF_6 (200 mg) dissolved in water (2 mL) was added. The dark green precipitate was filtered, washed with water, and dried. The product was isolated as a mixture of isomers (**7**/**8** = 3:1) (64 mg, 93%). Isomer **7** was isolated pure via chromatography on alumina, eluting with acetone/4% MeOH: ^{1}H NMR (500 MHz, acetone-d_6): δ 11.95 (1H, d, J = 1.2 Hz; H3), 9.17

dx.doi.org/10.1021/ic4022905 | *Inorg. Chem.* 2014, 53, 912−921

(1H, s; H3), 8.92−8.83 (6H, m), 8.80 (1H, d, J = 8.0 Hz), 8.76 (1H, d, J = 5.2 Hz), 8.72 (1H, d, J = 8.0 Hz), 8.68 (1H, d, J = 8.0 Hz), 8.44−8.22 (10H, m), 8.07 (1H, dt, J = 8.0, 1.7 Hz), 8.04 (1H, d, J = 5.2 Hz), 7.99 (1H, dt, J = 8.0, 1.2 Hz), 7.97 (1H, d, J = 8.0 Hz), 7.78−7.64 (7H, m), 7.60 (1H, d, J = 5.2 Hz), 7.45 (1H, dt, J = 6.6, 1.2 Hz), 7.25 (1H, dt, J = 6.9, 1.2 Hz), 7.19 (1H, dt, J = 6.9, 1.2 Hz). Anal. Calcd. for $C_{49}H_{37}F_{18}IN_{11}P_3Ru_2{\cdot}2H_2O{\cdot}0.5$ acetone: C, 37.70; H, 2.76; N, 9.58. Found: C, 37.91; H, 2.35; N, 9.21.

Synthesis of ***9b***. $[Ru(\mathbf{4b})_2Cl_2]$ (161 mg, 0.297 mmol) was added to a hot suspension of 2,5-(1′,8′-naphthyrid-2′-yl)pyrazine (100 mg, 0.297 mmol) in ethylene glycol (10 mL), and the reaction was irradiated in a MW oven for 7 min (1 × 5 min, 1 × 2 min). The reaction was allowed to cool to room temperature, and NH_4PF_6 (400 mg) dissolved in water (3 mL) was added. The precipitate was filtered, washed with water, and dried. Chromatography on alumina, eluting first with CH_2Cl_2/acetone (1:1) and then acetone, and recrystallization from acetone/water afforded **9b** as a red solid (154 mg, 47%): ^{1}H NMR (500 MHz, acetone-d_6): δ 10.24 (1H, d, J = 1.2 Hz), 9.23 (1H, dd, J = 4.0, 2.3 Hz), 9.19 (1H, d, J = 8.6 Hz), 9.17 (1H, d, J = 1.2 Hz), 8.92 (1H, d, J = 8.6 Hz), 8.79 (1H, s), 8.71 (2H, AB pattern, J = 8.6 Hz), 8.69 (1H, s), 8.66−8.63 (2H, m), 8.58 (1H, s), 8.55 (1H, dd, J = 8.3, 2.3 Hz), 8.38 (1H, dd, J = 4.3, 2.3 Hz), 8.02 (1H, d, J = 5.7 Hz), 7.99 (1H, d, J = 5.7 Hz), 7.91−7.88 (2H, m), 7.72 (2H, dd, J = 8.0, 4.0 Hz), 7.61 (1H, dd, J = 5.7, 1.2 Hz), 7.47 (1H, dd, J = 5.7, 1.2 Hz), 7.26 (1H, dd, J = 5.7, 1.2 Hz), 7.23 (1H, dd, J = 5.7, 1.2 Hz), 2.83 (3H, s), 2.67 (3H, s), 2.50 (3H, s), 2.47 (3H, s). Anal. Calcd. for $C_{44}H_{36}F_{12}N_{10}P_2Ru{\cdot}H_2O$: C, 47.44; H, 3.41; N, 12.58. Found: C, 47.48; H, 3.04; N, 12.24.

Synthesis of ***9c***. A mixture of $[Ru(\mathbf{4d})_2Cl_2]$ (110.0 mg, 0.11 mmol), 2,5-(1′,8′-naphthyrid-2′-yl)pyrazine (46.6 mg, 0.14 mmol), and EtOH/water (3:1 v/v, 30 mL) was refluxed for 14 h. The solvent was evaporated; the residue was dissolved in water and filtered. NH_4PF_6 (400 mg) dissolved in water (3 mL) was added. The precipitate was filtered, washed with water, and dried. Chromatography on alumina, eluting with acetone, and recrystallization from acetone/water afforded **9c** as a red solid (123 mg, 72%): ^{1}H NMR (500 MHz, acetone-d_6): δ 10.37 (1H, d, J = 1.2 Hz), 9.53 (1H, d, J = 1.2 Hz), 9.28 (1H, d, J = 8.6 Hz), 9.20 (1H, dd, J = 4.0, 1.7 Hz), 9.00 (1H, d, J = 8.6 Hz), 8.95 (1H, d, J = 1.7 Hz), 8.89 (1H, d, J = 1.7 Hz), 8.78 (2H, AB pattern, J = 8.6 Hz), 8.76 (1H, d, J = 1.2 Hz), 8.71−8.69 (1H, m), 8.68 (1H, d, J = 1.7 Hz), 8.59 (1H, dd, J = 8.3, 2.3 Hz), 8.36 (1H, d, J = 5.7 Hz), 8.32 (1H, dd, J = 4.3, 2.3 Hz), 8.28 (1H, d, J = 5.7 Hz), 8.14 (1H, d, J = 5.7 Hz), 8.12 (1H, d, J = 5.7 Hz), 7.81 (1H, dd, J = 8.0, 4.0 Hz), 7.76 (1H, dd, J = 8.0, 4.0 Hz), 7.58 (1H, dd, J = 5.7, 1.7 Hz), 7.51 (1H, dd, J = 5.7, 1.7 Hz), 7.35 (2H, dd, J = 5.7, 1.7 Hz), 4.12−3.54 (8H, m), 1.58−1.00 (48H, m). Anal. Calcd. for $C_{68}H_{80}F_{12}N_{14}O_4P_2Ru{\cdot}2H_2O$: C, 51.55; H, 5.34; N, 12.38. Found: C, 51.71; H, 4.61; N, 12.00.

Synthesis of ***9d***. The same procedure as described for **9c** was followed using $[Ru(\mathbf{5a})_2Cl_2]{\cdot}2H_2O$ (200.0 mg, 0.35 mmol) and 2,5-(1′,8′-naphthyrid-2′-yl)pyrazine (147.9 mg, 0.44 mmol) to afford a red solid (250 mg, 65%): ^{1}H NMR (400 MHz, acetone-d_6): δ 10.34 (1H, d, J = 0.9 Hz), 9.30 (1H, d, J = 0.9 Hz), 9.28 (1H, d, J = 9.2 Hz), 9.14 (1H, dd, J = 4.1, 2.3 Hz), 8.95 (1H, d, J = 8.7 Hz), 8.94 (1H, dd, J = 7.6, 0.9 Hz), 8.86−8.80 (2H, m), 8.77 (2H, dt, J = 8.7, 0.9 Hz), 8.66 (2H, AB pattern, J = 8.2 Hz), 8.58 (1H, dd, J = 8.2, 1.8 Hz), 8.54 (1H, dd, J = 5.0, 0.9 Hz), 8.49 (1H, dd, J = 8.2, 1.8 Hz), 8.47−8.28 (6H, m), 7.98 (1H, dd, J = 4.1, 1.8 Hz), 7.93 (1H, dd, J = 8.2, 5.0 Hz), 7.88−7.82 (2H, m), 7.78 (1H, dd, J = 8.2, 5.5 Hz), 7.67 (1H, dd, J = 8.0, 4.1 Hz), 7.58 (1H, dd, J = 8.2, 4.1 Hz). Anal. Calcd. for $C_{44}H_{28}F_{12}N_{10}P_2Ru{\cdot}0.1KPF_6$: C, 47.78; H, 2.55; N, 12.66. Found: C, 48.11; H, 2.08; N, 12.73.

Synthesis of ***9e***. The same procedure as described for **9b** was followed using $[Ru(\mathbf{5b})_2Cl_2]$ (150.0 mg, 0.18 mmol) and 2,5-(1′,8′-naphthyrid-2′-yl)pyrazine (59.5 mg, 0.18 mmol) to afford a red solid (132 mg, 53%): ^{1}H NMR (500 MHz, acetone-d_6): δ 10.34 (1H, d, J = 1.2 Hz), 9.28 (1H, d, J = 8.6 Hz), 9.23 (1H, d, J = 1.2 Hz), 9.17−9.13 (2H, m), 9.03−8.93 (6H, m), 8.67−8.63 (2H, m), 8.61−8.57 (2H, m), 8.51−8.48 (2H, m), 8.03 (1H, dd, J = 4.3, 1.7 Hz), 8.01 (1H, dd, J = 8.9, 5.2 Hz), 7.95 (1H, dd, J = 8.6, 5.2 Hz), 7.94 (1H, dd, J = 8.6, 5.2 Hz), 7.88 (1H, dd, J = 8.6, 5.7 Hz), 7.68 (1H, dd, J = 8.0, 4.0 Hz), 7.59 (1H, dd, J = 8.0, 4.0 Hz). Anal. Calcd. for $C_{44}H_{24}Br_4F_{12}N_{10}P_2Ru{\cdot}1/2C_3H_6O$: C, 38.15; H, 1.90; N, 9.78. Found: C, 38.14; H, 1.54; N, 9.58.

Synthesis of ***10a***. A mixture of **9a** (66 mg, 0.064 mmol) and $[Ru(tpy)Cl_3]$ (29 mg, 0.064 mmol) in EtOH/water (3:1, 20 mL) in the presence of triethylamine (0.3 mL) was heated at reflux overnight. After reducing the volume, NH_4PF_6 (160 mg) was added, and the precipitate was collected and washed with water, and dried. Chromatography on alumina, eluting with CH_2Cl_2/acetone (1:1) followed by recrystallization from CH_2Cl_2/Et_2O afforded the chloro-complex as a dark solid (50 mg, 50%). This chloro-complex (50 mg, 0.032 mmol) and KI (80 mg, 0.5 mmol) in acetone/water (1:1) was heated at 90 °C for 2 d. After reducing the volume, NH_4PF_6 (100 mg) was added, and the precipitate was collected and washed with water, and dried. Chromatography on alumina, eluting with CH_2Cl_2/acetone/water (1:1:0.5) followed by recrystallization from CH_2Cl_2/Et_2O afforded dyad **10a** as a dark solid (33 mg, 62%): ^{1}H NMR (500 MHz, acetone-d_6): δ 12.51 (1H, s), 9.40 (1H, s), 8.96 (2H, AB pattern, J = 8.6 Hz), 8.87 (1H, d, J = 8.6 Hz), 8.86 (2H, d, J = 8.0 Hz), 8.83 (1H, d, J = 8.0 Hz), 8.81 (1H, d, J = 8.0 Hz), 8.76 (1H, d, J = 7.5 Hz), 8.72 (1H, d, J = 8.0 Hz), 8.68 (1H, dd, J = 8.3, 2.3 Hz), 8.62 (1H, d, J = 5.7 Hz), 8.59 (1H, d, J = 8.0 Hz), 8.56 (1H, d, J = 8.0 Hz), 8.42−8.22 (8H, m), 8.21 (1H, d, J = 5.7 Hz), 8.19 (1H, d, J = 4.6 Hz), 8.15 (1H, dt, J = 8.0, 1.2 Hz), 8.07 (1H, d, J = 5.2 Hz), 8.03 (1H, d, J = 9.2 Hz), 7.94 (1H, dt, J = 8.0, 1.2 Hz), 7.86 (1H, dt, J = 8.0, 1.2 Hz), 7.74 (1H, dd, J = 8.0, 4.0 Hz), 7.71 (1H, dt, J = 6.6, 1.7 Hz), 7.64 (1H, dt, J = 6.9, 1.2 Hz), 7.61−7.55 (2H, m), 7.51 (1H, dd, J = 8.0, 4.0 Hz), 7.49 (1H, d, J = 6.3 Hz), 7.33 (1H, dt, J = 6.3, 1.2 Hz), 7.05 (1H, dt, J = 6.9, 1.2 Hz). Anal. Calcd. for $C_{55}H_{39}IN_{13}Ru_2P_3F_{18}{\cdot}2C_3H_6O$: C, 41.58; H, 2.92; N, 10.33. Found: C, 42.06; H, 2.43; N, 10.50.

Synthesis of ***10b***. The same procedure as described for **10a** was followed using **9b** as the starting material to afford a dark brown solid in 48% overall yield: ^{1}H NMR (500 MHz, acetone-d_6): δ 12.45 (1H, s), 9.50 (1H, s), 8.94 (2H, AB pattern, J = 8.6 Hz), 8.86−8.80 (4H, m), 8.71 (1H, d, J = 6.3 Hz), 8.69 (1H, dd, J = 8.3, 2.3 Hz), 8.63 (1H, s), 8.58 (1H, s), 8.57 (2H, s), 8.53 (1H, d, J = 4.6 Hz), 8.41−8.36 (3H, m), 8.31 (1H, dd, J = 7.5, 2.3 Hz), 8.27 (1H, dd, J = 4.3, 2.3 Hz), 8.16 (1H, d, J = 5.7 Hz), 8.11 (1H, d, J = 9.2 Hz), 8.05 (1H, d, J = 5.7 Hz), 7.94 (1H, dt, J = 8.0, 1.7 Hz), 7.88 (1H, dt, J = 8.0, 1.7 Hz), 7.84 (1H, d, J = 5.7 Hz), 7.74 (1H, dd, J = 8.0, 4.6 Hz), 7.66 (1H, d, J = 5.7 Hz), 7.56 (1H, dd, J = 5.7, 1.2 Hz), 7.52 (1H, dd, J = 8.0, 4.0 Hz), 7.47 (1H, dd, J = 5.7, 1.2 Hz), 7.44 (1H, dd, J = 5.7, 1.2 Hz), 7.40−7.35 (2H, m), 7.04 (1H, dt, J = 5.7, 1.2 Hz), 2.68 (3H, s), 2.66 (3H, s), 2.60 (3H, s), 2.51 (3H, s). Anal. Calcd. for $C_{59}H_{47}F_{18}IN_{13}P_3Ru_2{\cdot}2/3CH_2Cl_2$: C, 40.75; H, 2.77; N, 10.35. Found: C, 40.88; H, 2.42; N, 9.97.

Synthesis of ***10c***. The same procedure as described for **10a** was followed using **9c** as the starting material to afford a green solid in 38% overall yield: ^{1}H NMR (500 MHz, acetone-d_6): δ 12.54 (1H, s), 9.34 (1H, s), 8.97 (2H, AB pattern, J = 8.7 Hz), 8.96 (1H, d, J = 1.4 Hz), 8.88 (1H, d, J = 1.4 Hz), 8.84 (2H, dd, J = 8.2, 1.8 Hz), 8.78 (1H, d, J = 1.4 Hz), 8.72 (1H, dd, J = 8.2, 1.8 Hz), 8.69 (1H, d, J = 1.4 Hz), 8.62−8.56 (3H, m), 8.44−8.36 (5H, m), 8.34 (1H, d, J = 5.5 Hz), 8.28 (1H, dd, J = 4.1, 1.8 Hz), 8.14 (1H, d, J = 6.0 Hz), 8.10 (1H, d, J = 5.0 Hz), 8.06 (1H, d, J = 8.7 Hz), 7.94 (1H, dt, J = 7.8, 1.4 Hz), 7.90 (1H, dt, J = 7.8, 1.4 Hz), 7.84 (1H, dd, J = 8.2, 4.1 Hz), 7.66 (1H, dd, J = 5.0 Hz), 7.60 (1H, dd, J = 6.0, 1.4 Hz), 7.56 (1H, dd, J = 5.7, 1.4 Hz), 7.53 (1H, dd, J = 8.2, 4.1 Hz), 7.46 (2H, dt, J = 5.7, 1.4 Hz), 7.31 (1H, dt, J = 5.7, 1.4 Hz), 7.18 (1H, dt, J = 5.7, 1.4 Hz), 4.22−3.58 (8H, m), 1.61−1.11 (48H, m). Anal. Calcd. for $C_{83}H_{91}F_{18}IN_{17}O_4P_3Ru_2$: C, 46.23; H, 4.26; N, 11.05. Found: C, 46.44; H, 3.74; N, 10.57.

Synthesis of ***10d***. The same procedure as described for **10a** was followed using **9d** as the starting material to afford a green solid in 11% overall yield: ^{1}H NMR (500 MHz, acetone-d_6): δ 12.58 (1H, s), 9.53 (1H, s), 9.18 (1H, dd, J = 5.2, 1.2 Hz), 9.00 (2H, AB pattern, J = 8.6 Hz), 8.98 (1H, dd, J = 8.6, 1.2 Hz), 8.88 (1H, dd, J = 8.6, 1.2 Hz), 8.86−8.77 (4H, m), 8.75 (1H, dd, J = 4.0, 1.2 Hz), 8.64−8.59 (2H, m), 8.57 (1H, d, J = 8.0 Hz), 8.51−8.44 (3H, m), 8.40 (1H, t, J = 8.0 Hz), 8.34 (2H, AB pattern, J = 8.6 Hz), 8.28−8.24 (4H, m), 8.22 (1H, dd, J = 5.2, 1.2 Hz), 8.05 (1H, dd, J = 4.0, 1.7 Hz), 8.04−7.95 (3H, m),

dx.doi.org/10.1021/ic4022905 | *Inorg. Chem.* 2014, 53, 912−921

7.90−7.84 (3H, m), 7.79 (1H, dd, J = 8.0, 5.2 Hz), 7.62 (1H, dd, J = 8.0, 4.0 Hz), 7.53 (1H, d, J = 6.3 Hz), 7.50 (1H, dd, J = 8.0, 4.6 Hz), 7.40 (1H, dt, J = 6.3, 1.7 Hz), 7.00 (1H, dt, J = 6.0, 1.7 Hz). Anal. Calcd. for $C_{59}H_{39}F_{18}IN_{13}P_3Ru_2$: C, 41.83; H, 2.32; N, 10.75. Found: C, 41.44; H, 1.90; N, 10.34.

Synthesis of ***10e***. The same procedure as described for **10a** was followed using **9e** as the starting material to afford a green solid in 42% overall yield. ^{1}H NMR (500 MHz, acetone-d_6): δ 12.61 (1H, s), 9.49 (1H, s), 9.24 (1H, d, J = 4.6 Hz), 9.16 (1H, dd, J = 8.6, 1.2 Hz), 9.06 (1H, dd, J = 8.6, 1.2 Hz), 9.00 (2H, AB pattern, J = 8.6 Hz), 8.99 (1H, dd, J = 8.6, 1.2 Hz), 8.87 (1H, dd, J = 5.2, 1.2 Hz), 8.85 (1H, d, J = 8.0 Hz), 8.82 (1H, d, J = 8.6 Hz), 8.66−8.56 (4H, m), 8.43−8.39 (2H, m), 8.27−8.22 (4H, m), 8.13−8.07 (3H, m), 8.00−7.93 (3H, m), 7.88−7.81 (3H, m), 7.62 (1H, dd, J = 8.0, 4.0 Hz), 7.53−7.49 (2H, m), 7.38 (1H, dt, J = 5.7, 1.7 Hz), 7.01 (1H, dt, J = 5.7, 1.2 Hz). Anal. Calcd. for $C_{59}H_{35}Br_4F_{18}IN_{13}P_3Ru_2{\cdot}0.5KI{\cdot}C_3H_6O$: C, 34.63; H, 1.92; N, 8.47. Found: C, 34.94; H, 1.59; N, 8.16.

Synthesis of ***11***. The complex was prepared following a literature method[7] and characterized by ^{1}H NMR (400 Hz, CD_3CN) 9.83 (1H, d, J = 0.9 Hz), 9.21 (1H, dd, J = 4.1, 2.3 Hz), 9.04 (1H, d, J = 8.7 Hz), 8.72 (1H, d, J = 8.7 Hz), 8.65 (1H, d, J = 8.7 Hz), 8.60 (1H, s), 8.59 (1H, d, J = 8.7 Hz), 8.52 (2H, t, J = 7.3 Hz), 8.46 (2H, dd, J = 8.2, 1.8 Hz), 8.34 (2H, t, J = 8.2 Hz), 8.1 (1H, dd, J = 4.1, 1.8 Hz), 8.08 (1H, dt, J = 7.8, 1.4 Hz), 8.03 (1H, dt, J = 7.8, 1.4 Hz), 8.01 (1H, dt, J = 7.8, 1.4 Hz), 7.92 (1H, dt, J = 7.8, 1.4 Hz), 7.78 (2H, t, J = 5.5 Hz), 7.71 (2H, t, J = 5.5 Hz), 7.68 (1H, dd, J = 8.2, 4.1 Hz), 7.57 (1H, dd, J = 8.2, 4.1 Hz), 7.42 (1H, ddd, J = 7.4, 5.8, 1.4 Hz), 7.37 (1H, ddd, J = 7.4, 5.8, 1.4 Hz), 7.27 (1H, ddd, J = 7.4, 5.8, 1.4 Hz), 7.24 (1H, ddd, J = 7.4, 5.8, 1.4 Hz).

Synthesis of ***12***. A mixture of **11** (32 mg, 0.032 mmol), [Ru(tpy)Cl_3] (15 mg, 0.034 mmol), LiCl (100 mg), EtOH 10 mL, and water (5 mL) was refluxed for 8 h, followed by the addition of NH_4PF_6 (162 mg, 1.0 mmol) to produce a precipitate. The solid was collected and purified by chromatography on alumina eluting with MeOH/CH_2Cl_2 (1−2%) to afford a green fraction. Removal of the solvents yielded a green solid (17 mg, 34%). This chloro-complex (11 mg, 0.007 mmol) was combined with KI (300 mg), acetone (10 mL), and water (10 mL) and heated to reflux for 2 d. Acetone was removed by evaporation, and excess NH_4PF_6 was added to produce a precipitate that was collected by filtration and washed with cold water to give a dark solid (9 mg, 78%): ^{1}H NMR (400 MHz, CD_3CN) 11.05 (1H, s), 9.71 (1H, s), 9.18 (1H, d, J = 8.7 Hz), 8.93 (1H, d, J = 8.7 Hz), 8.82 (1H, d, J = 8.2 Hz), 8.47−8.51 (3H, m), 8.40 (4H, t, J = 7.3 Hz), 8.36 (1H, d, J = 7.8 Hz), 8.28 (1H, d, J = 8.2 Hz), 8.15−8.25 (5H, m), 8.12 (1H, dd, J = 4.1, 1.8 Hz), 8.05 (2H, dt, J = 7.8, 1.4 Hz), 8.01 (1H, dt, J = 8.0, 1.4 Hz), 7.93 (1H, d, J = 5.5 Hz), 7.83−7.88 (3H, m), 7.79 (1H, dt, J = 7.8, 1.4 Hz), 7.73 (1H, dt, J = 7.8, 1.4 Hz), 7.70 (1H, d, J = 6.0 Hz), 7.61 (1H, dd, J = 8.2, 4.1 Hz), 7.34−7.45 (4H, m), 7.24 (1H, dt, J = 5.6, 1.2 Hz), 7.18 (1H, dt, J = 5.5, 1.4 Hz), 6.85−6.90 (2H, m).

X-ray Structure Determination of 10a(I)$_3$·4CH$_3$CN. All measurements were made with a Bruker DUO platform diffractometer equipped with a 4K CCD APEX II detector. A hemisphere of data (1519 frames at 6 cm detector distance) was collected using a narrow-frame algorithm with scan widths of 0.30° in ω and an exposure time of 25 s/frame. The data were integrated using the Bruker-Nonius SAINT program, with the intensities corrected for Lorentz factor, polarization, air absorption, and absorption due to variation in the path length through the detector faceplate. A ψ-scan absorption correction was applied based on the entire data set. Redundant reflections were averaged. Final cell constants were refined using 7866 reflections having $I > 10\sigma(I)$, and these, along with other information pertinent to data collection and refinement, are listed in Supporting Information, Table S1. The Laue symmetry was determined to be 2/m, and from the systematic absences noted the space group was shown unambiguously to be $P2(1)/n$. The main diruthenium cation was found to consist of two different geometric isomers crystallizing on the same site, distinguished by the way the two bidentate bpy ligands attach to Ru2. The population factors refined to approximately 87%:13%. This distortion in the shape of the cation caused concomitant disorder in the surrounding anions and solvent molecules, making the overall structural model extremely complicated. It was also noted that the tpy ligand is disordered; however, this was not pursued since this disorder was not deemed to be critical to the interpretation of the crystal structure. Analysis of the bulk material showed indications of a small ammount of PF_6^- anion present replacing I^-; however, because of the massive disorder in each of the three anion sites in the data crystal, it was impossible to determine if any PF_6^- was present. So the assumption was made that this crystal contains only iodide anions. The disordered acetonitrile solvent molecules were treated as ideal rigid bodies, with population factors estimated based on comparison of isotropic displacement parameters. The assumption was made that each solvent site is 100% occupied, although, in fact, it is quite possible that some significant amount of solvent may have been lost during crystal handling. One of the orientations of the fourth solvent site did not behave well as a rigid body, so all atoms were refined independently. It is possible that these disjointed atoms actually belong to two different orientations that could not be clearly identified.

■ ASSOCIATED CONTENT

Ⓢ Supporting Information

X-ray crystallographic data for **10a(I)$_3$·4CH$_3$CN** in CIF format. ^{1}H NMR spectra for **7**, **9b−e**, **10a−e**, **11**, and **12**. This material is available free of charge via the Internet at http://pubs.acs.org.

■ AUTHOR INFORMATION

Corresponding Author

*E-mail: thummel@uh.edu.

Notes

The authors declare no competing financial interest.

■ ACKNOWLEDGMENTS

This work was funded by the Division of Chemical Sciences, Geosciences, and Biosciences, Office of Basic Energy Sciences of the U.S. Department of Energy through Grant DE-FG02-07ER15888. We also thank the Robert A. Welch Foundation (E-621) for support and Dr. James Korp for assistance with the X-ray determination.

■ REFERENCES

(1) (a) Zong, R.; Thummel, R. P. *J. Am. Chem. Soc.* **2005**, *127*, 12802−12803. (b) Deng, Z.; Tseng, H.-W.; Zong, R.; Wang, D.; Thummel, R. P. *Inorg. Chem.* **2008**, *47*, 1835−1848. (c) Jiang, Y.; Li, F.; Zhang, B.; Li, X.; Wang, X.; Huang, F.; Sun, L. *Angew. Chem., Int. Ed.* **2013**, *52*, 3398−3401. (d) Xu, Y.; Duan, L.; Tong, L.; Åkermark, B.; Sun, L. *Chem. Commun.* **2010**, 6506−6508. (e) Xu, Y.; Åkermark, T.; Gyollai, V.; Zou, D.; Eriksson, L.; Duan, L.; Zhang, R.; Åkermark, B.; Sun, L. *Inorg. Chem.* **2009**, *47*, 2717−2719. (f) Sens, C.; Romero, I.; Rodriguez, M.; Llobet, A.; Parella, T.; Benet-Buchholz, J. *J. Am. Chem. Soc.* **2004**, *126*, 7798−7799. (g) Mola, J.; Dinoi, C.; Sala, X.; Rodriguez, M.; Romero, I.; Parella, T.; Fontrodona, X.; Llobet, A. *Dalton Trans.* **2011**, *40*, 3640−3646.

(2) (a) Kaveevivitchai, N.; Zong, R.; Tseng, H.-W.; Chitta, R.; Thummel, R. P. *Inorg. Chem.* **2012**, *51*, 2930−2939. (b) Tseng, H.-W.; Zong, R.; Muckerman, J. T.; Thummel, R. *Inorg. Chem.* **2008**, *48*, 11763−11773. (c) Roeser, S.; Farràs, P.; Bozoglian, F.; Martínez-Belmonte, M.; Benet-Buchholz, J.; Llobet, A. *ChemSusChem* **2011**, *4*, 197−207. (d) Concepcion, J. J.; Jurss, J. W.; Norris, M. R.; Chen, Z.; Templeton, J. L.; Meyer, T. J. *Inorg. Chem.* **2010**, *49*, 1277−1279. (e) Concepcion, J. J.; Jurss, J. W.; Templeton, J. L.; Meyer, T. J. *J. Am. Chem. Soc.* **2008**, *130*, 16462−16463. (f) Concepcion, J. J.; Tsai, M.-K.; Muckerman, J. T.; Meyer, T. J. *J. Am. Chem. Soc.* **2010**, *132*, 1545−1557. (g) Cao, R.; Lai, W.; Du, P. *Energy Environ. Sci.* **2012**, *5*, 8134−8157. (h) Kärkäs, M. D.; Åkermark, T.; Johnston, E. V.; Karim, S. R.; Laine, T. M.; Lee, B.-L.; Åkermark, T.; Privalov, T.; Åkermark, B. *Angew. Chem., Int. Ed.* **2012**, *51*, 11589−11593. (i) Radaram, B.; Ivie, J.

A.; Singh, W. M.; Grudzien, R. M.; Reibenspies, J. H.; Webster, C. E.; Zhao, X. *Inorg. Chem.* **2011**, *50*, 10564−10571.
(3) (a) Farras, P.; Maji, S.; Benet-Buchholz, J.; Llobet, A. *Chem.—Eur. J.* **2013**, *19*, 7162−7172. (b) Song, W.; Glasson, C. R. K.; Hanlin, L.; Hanson, K.; Brennaman, M. K.; Concepcion, J. J.; Meyer, T. J. *J. Phys. Chem. Lett.* **2011**, *2*, 1808−1813. (c) Norris, M. R.; Concepcion, J. J.; Harrison, D. P.; Binstead, R. A.; Ashford, D. L.; Fang, Z.; Templeton, J. L.; Meyer, T. J. *J. Am. Chem. Soc.* **2013**, *135*, 2080−2083. (d) Frischmann, P. D.; Mahata, K.; Wurthner, F. *Chem. Soc. Rev.* **2013**, 1847−1870. (e) Ashford, D. L.; Stewart, D. J.; Glasson, C. R.; Binstead, R. A.; Harrison, D. P.; Norris, M. R.; Concepcion, J. J.; Fang, Z.; Templeton, J. L.; Meyer, T. J. *Inorg. Chem.* **2012**, *51*, 6428−6430. (f) Hamelin, O.; Guillo, P.; Loiseau, F.; Boissonnet, M.-F.; Menage, S. *Inorg. Chem.* **2011**, *50*, 7952−7954.
(4) Kaveevivitchai, N.; Chitta, R.; Zong, R.; El Ojaimi, M.; Thummel, R. P. *J. Am. Chem. Soc.* **2012**, *134*, 10721−10724.
(5) (a) Wasylenko, D. J.; Ganesamoorthy, C.; Henderson, M. A.; Kolvisto, B. D.; Osthoff, H. D.; Berlinguette, C. P. *J. Am. Chem. Soc.* **2010**, *132*, 16094−16106. (b) Wasylenko, D. J.; Ganesamoorthy, C.; Kolvisto, B. D.; Henderson, M. A.; Berlinguette, C. P. *Inorg. Chem.* **2010**, *49*, 2202−2209.
(6) (a) Case, F. H.; Koft, E. *J. Am. Chem. Soc.* **1959**, *81*, 905−906. (b) Tsubomura, T.; Enoto, S.; Endo, S.; Tamane, T.; Matsumoto, K.; Tsukuda, T. *Inorg. Chem.* **2005**, *44*, 6373−6378.
(7) Brown, D.; Muranjan, S.; Thummel, R. P. *Eur. J. Inorg. Chem.* **2003**, 3547−3553.
(8) (a) Zong, R.; Naud, F.; Segal, C.; Burke, J.; Wu, F.; Thummel, R. *Inorg. Chem.* **2004**, *43*, 6195−6202. (b) Boyer, J. L.; Polyansky, D.; Szalda, D. J.; Zong, R.; Thummel, R. P.; Fujita, E. *Angew. Chem., Int. Ed.* **2011**, *50*, 12600−12604.
(9) (a) Schulz, M.; Hirschmann, J.; Draksharapu, A.; Bindra, G. S.; Soman, S.; Paul, A.; Groarke, R.; Pryce, M. T.; Rau, S.; Browne, W. R.; Vos, J. G. *Dalton Trans.* **2011**, *40*, 10545−10552. (b) Bindra, G. S.; Schulz, M.; Paul, A.; Soman, S.; Groarke, R.; Inglis, J.; Pryce, M. T.; Browne, W. R.; Rau, S.; Maclean, B. J.; Vos, J. *Dalton Trans.* **2011**, *40*, 10812−10814.
(10) Bock, C. R.; Connor, J. A.; Gutierrez, A. R.; Meyer, T. J.; Whitten, D. G.; Sullivan, B. P.; Nagle, J. K. *J. Am. Chem. Soc.* **1979**, *101*, 4815−4824.
(11) Denti, G.; Campagna, S.; Sabatino, L.; Serrni, S.; Ciano, M.; Balzani, V. *Inorg. Chem.* **1990**, *29*, 4750−4758.
(12) Matsumura-Inoue, T.; Tanabe, M.; Minami, T.; Ohashi, T. *Chem. Lett.* **1994**, 2443−2446.
(13) Sullivan, B. P.; Calvert, J. M.; Meyer, T. J. *Inorg. Chem.* **1980**, *19*, 1404−1407.
(14) Sullivan, B. P.; Salmon, D. J.; Meyer, T. J. *Inorg. Chem.* **1978**, *17*, 3334−3341.
(15) Qu, P.; Thompson, D. W.; Meyer, G. J. *Langmuir* **2000**, *16*, 4662−4671.
(16) Hara, M.; Waraksa, C. C.; Lean, J. T.; Lewis, B. A.; Mallouk, T. E. *J. Phys. Chem. A* **2000**, *104*, 5275−5280.